Dual intra- and extracellular release of monomethyl auristatin E from a neutrophil elastase-sensitive antibody-drug conjugate

Imene Ait Mohamed Amar, Steve Huvelle, Emmanuel Douez, Stéphanie Letast, Sylvain Henrion, Marie-Claude Viaud-Massuard, Nicolas Aubrey, Emilie Allard-Vannier, Nicolas Joubert, Caroline Denevault-Sabourin

Dual intra- and extracellular release of Monomethyl Auristatin E from a neutrophil elastase-sensitive antibody-drug conjugate

Imene Ait Mohamed Amar [a,1], Steve Huvelle [a,1], Emmanuel Douez [b], Stéphanie Letast [a], Sylvain Henrion [a], Marie-Claude Viaud-Massuard [a], Nicolas Aubrey [c], Emilie Allard-Vannier [b], Nicolas Joubert [a,2,*], Caroline Denevault-Sabourin [a,2,*].

[a] EA 7501 GICC, Team IMT, University of Tours, F-37032 Tours, France
[b] EA 6295 NMNS, University of Tours, F-37200 Tours, France
[c] UMR 1282 ISP, Team BioMAP, University of Tours-INRAE, F-37200 Tours, France.
[1] These authors contributed equally to this work.
[2] These authors contributed equally to this work.

* Corresponding authors, Innovation Moléculaire et Thérapeutique, EA7501 GICC, University of Tours, UFR de Médecine, Bâtiment Vialle, 7ème étage, 10 Bd Tonnellé, BP 3223, 37032 TOURS Cedex 01, France. Tel.: +33 2 47367231.
E-mail address: caroline.sabourin@univ-tours.fr (C. Denevault-Sabourin) and nicolas.joubert@univ-tours.fr (N. Joubert).

Abstract

Antibody-drug conjugates (ADCs) are targeted therapies, mainly used in oncology, consisting in a three-component molecular architecture combining a highly potent drug conjugated *via* a linker onto a monoclonal antibody (mAb), designed for the selective delivery of the drug to the tumor site. The linker is a key component, defining the ADC stability and mechanism of action, and particularly the drug release strategy. In this study, we have developed and synthesized a cleavable linker, which possesses an Asn-Pro-Val (NPV) sequence sensitive to the human neutrophil elastase (HNE), overexpressed in the tumor microenvironment. This linker permitted the site-specific conjugation of the cell-permeable drug, monomethyl auristatin E (MMAE), onto trastuzumab, using a disulfide re-bridging technology. The resulting ADC was then evaluated *in vitro*. This conjugate demonstrated retained antigen (Ag) binding affinity

and exhibited high subnanomolar potency against Ag-positive tumor cells after internalization, suggesting an intracellular mechanism of linker cleavage. While no internalization and cytotoxic activity of this ADC was observed on Ag-negative cells in classical conditions, the supplementation of exogenous HNE permitted to restore a nanomolar activity on these cells, suggesting an extracellular mechanism of drug release in these conditions. This *in vitro* proof of concept tends to prove that the NPV sequence could allow a dual intra- and extracellular mechanism of drug release. This work represents a first step in the design of original ADCs with a new dual intra- and extracellular drug delivery system and opens the way to further experimentations to evaluate their full potential *in vivo*.

Keywords

Extracellular release; antibody-drug conjugate (ADC); human neutrophil elastase (HNE); anticancer targeted therapy; cancer; tumor targeting.

Abbreviations[1]

[1] ADC, antibody-drug conjugate; HNE, human neutrophil elastase; IC_{50}, 50% inhibitory concentration; NPV trigger, asparagine proline. valine trigger;

1. Introduction

Immunoconjugates, and particularly, antibody-drug conjugates (ADCs) have been extensively developed over the last four decades, with applications, mainly in cancer therapy [1,2]. An ADC is a targeted therapy, resulting from the conjugation of a potent agent (also called payload or drug), chemically attached through a linker to a monoclonal antibody (mAb), combining the targeting specificity of the mAb with the high activity of a small molecule drug [3–5]. To date, eleven ADCs have been approved by the Food and Drug Administration (FDA), while around 80 are currently under clinical development [6].

The most explored strategy for ADC design consists in cancer cells targeting, using mAb directed against internalizing antigens (Ag) of the cancer cells surface. After specific Ag binding, these conjugates usually undergo an antigen-mediated internalization and release their cytotoxic agent or metabolite in the lysosomal compartment, after, respectively, cleavage of their linker (cleavable linker) or complete ADC digestion (non-cleavable linker) [7].

Non-cleavable linkers demonstrate a high plasma stability, but they are also dependent on efficient internalization and intracellular ADC degradation to release an active metabolite [8]. Moreover, due to its charged character at physiological pH, this active metabolite cannot cross biological membranes to achieve a bystander effect on neighboring cells. Therefore, ADCs with non-cleavable linkers lead essentially to the death of Ag-positive tumor cells [9,10]. This strategy, while effective, remains nevertheless restricted to homogeneous tumors, with high level of expression of the targeted Ag. Moreover, the dependence upon direct cell-surface Ag internalization and intracellular processing of these ADCs to be effective make them sensitive to many resistance mechanisms: decrease of target Ag expression, defects in ADC binding, internalization, trafficking or recycling, reduction of lysosomal proteolytic activity, or impaired lysosomal release due to reduced expression of lysosomal transporters [11–16].

Cleavable linkers exploit specific features of the tumor endosomal or lysosomal environment (*e.g.* acidic conditions, high glutathione (GSH), glucuronidase or protease levels) for the efficient intracellular release of the free drug (for a review, see [1,7]). The

capacity of the released free payload to achieve a bystander killing effect depends on its permeability and its ability to diffuse through biological membranes out of the tumor cell, and enter surrounding cells, leading to death of both Ag-positive and Ag-negative tumor cells [17]. This property permits the treatment of tumors with heterogeneous levels of target Ag expression. Moreover, there is emerging evidence that some of these ADCs with particular cleavable linker/cell-permeable drug combinations can kill cells through mechanisms independently of internalization, and that internalization may be non-essential for their anti-tumor activity [17]. This particularity can be useful to circumvent resistance mechanisms related to ADC endocytosis and intracellular processing. Thus, acid-labile, GSH- or protease (cathepsin B)-sensitive linkers, while being sensitive to tumor lysosomal environment can also be cleaved extracellularly in the tumoral microenvironment [18–25]. Indeed tumoral lysosomal compartment and tumoral microenvironment share characteristic features as acidic pH and high GSH and proteases levels, allowing a dual intra- and extracellular mechanism of release of the active payload from these linkers. In the case of a diffusible drug, the payload extracellularly released can penetrate neighboring cells and achieve bystander tumor cell killing whatever the level of cell target Ag expression and independently of ADC internalization.

If acid-labile and GSH-sensitive linkers show limited plasma stability and short half-lives, protease-responsive linkers demonstrate enhanced stability and reduced off-target toxicity and represent an important step in ADC development [26,27]. However, expression, concentration and activity of lysosomal proteases differ between tumors as well as their concentration in the tumor microenvironment [11]. It is consequently worthwhile to widen the scope of protease-sensitive linkers for ADCs.

In this context, a tripeptide Asn-Pro-Val (NPV) sequence was identified in 2002, as a specific substrate of human neutrophil elastase (HNE) [28]. HNE is a serine protease, stored in azurophilic granules of neutrophils, which plays a key role in innate immunity and physiologic inflammation [29]. Besides being released in the extracellular space during infection or inflammation, HNE is also secreted by infiltrating neutrophils and granulocytic myeloid derived suppressor cells in the tumor microenvironment, promoting primary tumor growth and secondary organ metastasis. Thus, cancers are characterized by significantly elevated levels of HNE, especially in the stroma [29],

which makes HNE an interesting protease for protease-sensitive linkers development. Interesting proofs of concept, using an NPV sequence for the development of original small molecule-drug conjugates (SMDCs), demonstrated that this NPV trigger could be cleaved extracellularly in the presence of HNE. Moreover, these studies showed that this peptide sequence could also be digested by rat-liver lysosome extracts, which can be of interest for a dual intra- and extracellular mechanism of release [30]. To the best of our knowledge, no ADC bearing this sequence have been reported in the literature. These findings prompted us to explore the applicability of NPV linkers in the design of new ADCs. We report herein the development and evaluation of the first HNE-sensitive ADC.

2. Results and discussion

2.1. Design of linker-drug

In this study, the FDA-approved trastuzumab, which targets the human epidermal growth factor receptor 2 (HER2), was chosen as a model antibody. The linker contains the NPV-PABC-MMAE sequence, with NPV, as the HNE-sensitive trigger, and where the PABC acts as a self-immolative spacer, to free the potent cytotoxic drug monomethyl auristatin E (MMAE), according to the mechanism depicted in Fig. 1. MMAE is able to diffuse through biological membrane, an essential property to achieve a bystander killing effect, necessary in the case of a dual intra- and extracellular mechanism of release. The conjugation of the linker on trastuzumab was realized, by a site-specific conjugation method, using a (diphenylthiomaleimido)caproic acid (diSPhMC) head for disulfide stapling on cysteine residues. This methodology allows the re-bridging of previously reduced interchain disulfide bonds, leading to stable and homogeneous immunoconjugates [31–38], and limiting the formation of low and high DAR species, known to compromise the ADC therapeutic window in auristatin-containing ADCs [39].

2.2. Chemistry

For the preparation of the linker-drug, the activated site-specific bioconjugation head **2** and the linker-payload fragment **8** were needed. These building blocks were synthesized separately, as described in Scheme 1. The preparation of the 6-(3,4-bis(phenylthio)maleimido)caproic acid **1** was performed according to a previously described literature procedure [35], and then converted into the reactive pentafluorophenyl (Pfp) ester **2**.

The synthesis of linker-payload fragment **8** was achieved in five steps from commercial protected amino acids. Briefly, starting from Asn(Trt)-OH, Fmoc-Pro-OH and Fmoc-Val-OH, the tripeptide **3** was easily obtained, using an automated single channel microwave peptide synthesizer. After coupling reaction of intermediate **3** with 4-(((*tert*-butyldimethylsilyl)oxy)methyl)aniline, followed by TBDMS group deprotection, the resulting compound **5** was activated with *p*-nitrophenyl chloroformate to give carbonate **6**. The latter underwent a coupling reaction with MMAE·TFA salt, providing intermediate **7**, which was then deprotected, to remove the Fmoc group, and then coupled with Pfp ester **2**, leading to the desired linker-drug diSPhMC-NPV-PABC-MMAE **9**.

2.3. Bioconjugation and characterization of TTZ-MC-NPV-MMAE conjugate

The bioconjugation of linker-drug **9** on the internalizing anti-HER2 humanized antibody, trastuzumab (IgG1), was performed in two steps (Fig. 1). Interchain disulfide bridges of trastuzumab were first mildly reduced, using 6 eq of tris(2-carboxyethyl)phosphine (TCEP) to release the free thiols, and then 6 eq of compound **9** were added to bridge the cysteine residues. This sequence was repeated, using 3 eq of TCEP and linker-drug **9**. The mixture was finally purified by size-exclusion chromatography on a Superdex 75 column, leading to TTZ-MC-NPV-MMAE (**10**).

The characterization of TTZ-MC-NPV-MMAE **10** was realized by denaturing high-resolution mass spectrometry (HRMS) (Supporting Information Fig. S1). The drug-to-antibody ratio (DAR) of conjugate **10** was then determined by HRMS (Supporting Information Fig. S1) and by hydrophobic interaction chromatography (HIC) (Supporting Information Fig. S2). Both methods demonstrated an average DAR of 3.5, with, in HIC, more than 50% of DAR 4 species, an optimal DAR for MMAE-containing

ADCs [39,40]. As expected when performing disulfide stapling with a bioconjugation head, unconjugated mAb (DAR 0) or species with high DAR (> 5) were not observed. Finally, the aggregation profile of conjugate **10** was studied by size-exclusion chromatography (SEC). These data revealed no obvious aggregation and suggested that TTZ-MC-NPV-MMAE was composed of more than 91% of monomer (Supporting Information Fig. S3).

2.4. Binding affinity of TTZ-MC-NPV-MMAE conjugate

In order to test whether our new linker affected antigen recognition, the HER2 binding properties of TTZ-MC-NPV-MMAE (**10**) was then evaluated by enzyme-linked immunosorbent (ELISA) assay in comparison to the non-conjugated native antibody, trastuzumab. The ADC **10** was found to have retained binding to HER2, which was comparable to trastuzumab (Fig. 2). These dose-response experiments showed that the MC-NPV-MMAE linker-drug had a minimal impact on antigen recognition.

2.5. Enzymatic cleavage of TTZ-MC-NPV-MMAE conjugate

The enzymatic cleavage of TTZ-MC-NPV-MMAE (**10**) in presence of HNE was further evaluated, using denaturing mass spectrometry for samples analysis. Quantitative NPV linker cleavage was observed within 2 h (Supporting Information Fig. S4), confirming that our new linker was cleaved by the enzyme. The subsequent MMAE release from the linker in presence of HNE was then studied, using high performance liquid chromatography (HPLC) for analysis. On HNE addition, the NPV linker was cleaved and only free MMAE was observed, which indicates both cleavage and efficient self-immolation of the PABC unit (Supporting Information Fig. S5).

2.5. Internalization of TTZ-MC-NPV-MMAE conjugate

The internalization of TTZ-MC-NPV-MMAE (**10**) was then evaluated by confocal fluorescence microscopy and flow cytometry studies (FACS analysis) on two human cell lines: SK-BR-3, a HER2 overexpressing breast cancer cell line (HER2+), and

MDA-MB-231, a highly aggressive triple-negative breast cancer (TNBC) cell line, characterized by a lack of HER2 gene amplification (HER2-). As shown in Fig. 3, after 48 h of exposure, a fair accumulation of ADC **10** in the intracellular compartments of HER2-positive SK-BR-3 cells was detected, suggesting an efficient receptor-mediated endocytosis of ADC **10** in these cells (Fig. 3A). On the contrary, no significant intracellular uptake was observed in HER2-negative MDA-MB-231 cells (Fig. 3B). Moreover, a quantitative evaluation of endocytosis was performed by flow cytometry after the pre-incubation of ADC **10** with protein L coupled with phycoerythrin (ppL-PE), used as an intracellular tracer (Fig. 3C). The non-specific uptake of ppL-PE has been quantified and was considered negligible regarding the obtained values (28 arbitrary units (AU) for SK-BR-3 HER2+ cells *versus* 14 AU for MDA-MB-231 HER2- cells). Results showed that there is a large increase of the uptake of ADC **10** on HER2+ cancer cells compared to HER2- cells as the mean fluorescence intensity (MFI) increase from 16 to 250 on MDA-MB-231 and SK-BR-3 cell lines, respectively. The presence of HNE do not alter this entry as the MFI are unchanged for the cells incubated with ADC **10** in the presence of the enzyme.

2.6. In vitro antitumor activity of TTZ-MC-NPV-MMAE conjugate

Antiproliferative activity of TTZ-MC-NPV-MMAE (**10**) was then tested *in vitro*, in presence or absence of HNE supplementation in the culture medium at a nontoxic concentration (50 nM), on SK-BR-3 (HER2+) and MDA-MB-231 (HER2-) cell lines. Cytotoxic effects were evaluated using a luminescent CellTiter-Glo proliferation assay, based on ATP quantification (Promega Wiscousin, USA) [41]. Trastuzumab and free MMAE were used as controls.

As shown in Table 1, in absence of HNE supplementation, ADC **10** demonstrated a highly potent cytotoxic activity on HER2+ SK-BR-3 cells (IC_{50} of 0.23 ± 0.08 nM) (Table 1, entry 1), in which a massive intracellular ADC uptake was detected, suggesting an intracellular mechanism of linker cleavage. These results are consistent with the literature data [30] that reported evidence of NPV linker digestion by lysosome extracts, permitting the intracellular lysosomal cleavage of the NPV linker after ADC internalization (Fig. 5).

The addition of HNE in the culture medium led to a very similar cell proliferation inhibition profile of ADC **10** on SK-BR3-cells (Fig. 4 and Table 1, entry 2), suggesting that the possibility of a dual intra- and extracellular mechanism of release does not affect the global activity of ADC **10** on Ag-positive tumor cells.

In absence of HNE supplementation, ADC **10** did not display significant cytotoxicity on HER2- MDA-MB-231 cells (IC_{50} > 1000 nM), whereas free MMAE inhibited cell proliferation at subnanomolar concentrations (IC_{50} of 0.53 ± 0.06 nM) (Table 1, entries 1 and 4). These results demonstrated that, without HNE addition, ADC **10** is inactive on target Ag-negative tumor cells, where no ADC internalization by receptor-mediated endocytosis was observed, tending to prove that, in these conditions, neither intra- nor extracellular linker cleavage can occur to release the free MMAE.

In contrast, after addition of exogenous HNE, ADC **10** significantly inhibited MDA-MB-231 cell growth at nanomolar concentrations (IC_{50} of 47.5 ± 7.9nM) (Table 1, entry 2), suggesting an extracellular cleavage of the HNE-sensitive linker, followed by passive diffusion of the free MMAE released, across the cell membrane of neighboring cells, allowing a cytotoxic activity on these Ag-negative cancer cells (Fig. 5).

3. Conclusion

In the course of ADCs development, the nature of the linker, connecting the highly potent drug to the mAb is a key component to consider, requiring careful design. The emergence of protease-sensitive linkers has revolutionized this field of research, enhancing linker stability and cleavage selectivity to improve ADC therapeutic index. One of the well-established hallmarks of cancers is the presence of an inflammatory microenvironment associated with tumor-infiltrating immune cells, secreting high levels of proteases [42], such as HNE, which can be exploited to trigger a selective drug release in the tumor microenvironment. In this study, we used the HNE-sensitive NPV sequence to design an ADC with a new dual intra- and extracellular drug delivery system. This ADC was able to kill Ag-positive tumor cells after internalization with IC_{50} in the subnanomolar range. While no internalization and cytotoxic activity of this ADC was observed on Ag-negative cells in classical conditions, the addition of exogenous HNE, known to be overexpressed in the tumor microenvironment, permitted

to restore a nanomolar activity on these cells, suggesting an extracellular mechanism of drug release in these conditions, and a subsequent bystander killing effect. These studies tend to prove that the NPV sequence could allow a dual intra- and extracellular mechanism of drug release, which could be of great interest in heterogeneous tumors with various levels of cell target Ag expression or to circumvent some issues related to the dependence of ADCs upon cell-surface Ag internalization and intracellular processing. Moreover, the diffusion of the free cytotoxic drug released in the tumor microenvironment could trigger the death of a large variety of Ag-negative tumor cells or cancer-associated cells, like tumor endothelial cells, which may be of interest in the field of cancer therapy. This *in vitro* proof of concept remains to be confirmed *in vivo* in mouse models. As high levels of HNE are observed in many cancers, we believe that this strategy could be applied in the design of ADCs directed against a great variety of tumor types.

5. Experimental section

5.1. General remarks

All solvents were anhydrous reagents from commercial sources. Unless otherwise noted, all chemicals and reagents were obtained commercially and used without purification. TFA salt of MMAE was purchased from Levena Biopharma (#T1004).
Known compounds were prepared according to literature procedures: 4-(((*tert*-butyldimethylsilyl)oxy)methyl)aniline [43], compound **1** [35].
Trastuzumab (Ontruzant®, Samsung Bioepis) was kindly provided by the Hospital Pharmacy of the Tours Teaching Hospital.
Microwave heating and peptide synthesis were carried out with a single-mode Initiator Alstra unit (Biotage). Thin layer chromatography (TLC) was performed using commercial pre-coated aluminium sheets silica gel (60 Å, F254; Merk) and revealed under 254 nm UV lamp. Column chromatography was carried out on an ISCO purification unit, Combi Flash RF 75 PSI, with Redisep flash silica gel columns (60 Å, 230-400 mesh, grade 9385). Purity of final compounds was determined by high performance liquid chromatography (HPLC). HPLC analysis were carried out with a LaChrom Elite system [Hitachi L-2130 (pump), L-2200 (autosampler) and L-2400 (UV-detector)], with a UV detection at 254 nm at 25 °C, and a XBridge C-18 column (250 × 10 mm, 4 µm, 135 Å); elution was performed with 0.1% trifluoroacetic acid (TFA) in water (solvent A), and 0.1% TFA in acetonitrile (MeCN) (solvent B), with a gradient from 20 to 100% of B over 35 minutes with a flow rate of 1 $mL.min^{-1}$; injection was realized at 1 mg/mL in DMSO (10 µL). Final compounds were obtained in a purity ≥ 95%. Semi-preparative HPLC was carried out on a Gilson PLC 2050 system [ARMEN V2 (pump), ECOM TOYDAD600 (UV-detector)], with a UV detection at 254 nm at 25 °C, and a Waters XBridge™ C-18 column (250 mm x 19 mm, 5 µm); elution was performed with 0.1 % TFA in water (solvent A), and 0.1% TFA in MeCN (solvent B); with a gradient from 20 to 100% of B over 32 min and then 100% of B for 6 min at 17.1 mL/min. NMR spectra were recorded at 300 MHz (^1H) on a Bruker Avance (300 MHz) spectrometer, and at 400 MHz (^1H) on a Bruker AVANCE NEO (400 MHz) spectrometer. The chemical shifts are reported in parts per million (ppm, δ) relative to

residual deuterated solvent peaks. The abbreviations s = singlet, d = doublet, t = triplet, q = quadruplet, m = multiplet and bs = broad signal were used throughout.

For small-molecule mass analysis, high-resolution accurate mass spectrometry measurements (HRMS) were performed using an Acquity UPLC H-Class system hyphenated to a Vion IMS Q-Tof mass spectrometer (Waters). Before MS analysis, 1 ng of sample was injected onto a BEH C18 column (2.1 × 50 mm, 1.7 μm) heated to 50 °C. A 6 min gradient from 5% to 90% solvent B was applied with a 0.5 mL/min flow rate to elute the sample (solvent A: H_2O + 0.1% formic acid; solvent B: MeCN + 0.1% formic acid). MS data were acquired in positive mode with an ESI source over a 50-1400 *m/z* window with 0.2 Hz scan rate and collision energy ramp from 20 to 40 eV. Data were processed using UNIFI software version 1.9.4.

5.2. Chemistry

*5.2.1. Perfluorophenyl 6-(3,4-bis(phenylthio)maleimido)hexanoate (**2**)*

6-(3,4-bis(phenylthio)maleimido)caproic acid (46.6 mg, 0.11 mmol) and pentafluorophenol (20.1 mg, 0.11 mmol) were dissolved in 1.5 mL of dry tetrahydrofuran (THF) and stirred at ice bath temperature. *N*,*N*'-dicyclohexylcarbodiimide (DCC) (22.5 mg, 0.11 mmol) was then added to the solution at 0 °C. The resulting mixture was stirred overnight at room temperature. The solvent was then removed under reduced pressure, and the residue was dissolved in dichloromethane (DCM) and filtrated. The crude was finally purified by column chromatography using cyclohexane with ethyl acetate gradient (0-10%) as eluent to afford compound **2** (58.6 mg, 91%) as a yellow oil.

^{1}H NMR (300 MHz, $CDCl_3$) δ 7.38-7.22 (m, 10H), 3.57 (t, 2H, J = 7.5 Hz), 2.69 (t, 2H, J = 7.5 Hz), 1.82 (dt, 2H, J = 15.0, 7.5 Hz), 1.69 (dt, 2H, J = 15.0, 7.5 Hz), 1.50-1.30 (m, 2H). HRMS (ESI) *m/z*: [M+H]+ calcd for $C_{28}H_{21}F_5NO_4S_2$, 594.0827; found 594.0823.

*5.2.2. Fmoc-Asn-Pro-Val-OH (**3**)*

Into a specific microwave vial was introduced a Fmoc-Val-OH loaded Wang resin (700 mg, 0.7 mmol/g, 0.49 mmol). The resin was activated by DCM (32 mL) and the solvent

was removed by filtration. Then, piperidine (11.5 mL, 20% in DMF) was introduced. The suspension was shacked smoothly at room temperature and filtrated to give the deprotected Val-OH loaded on resin. Then, *N*,*N*′-diisopropylcarbodiimide (DIC) (353.5 µL, 1.96 mmol), Oxyma (310.5 mg, 1.96 mmol, 4.5 M in *N*-methyl-2-pyrrolidone) and Fmoc-Pro-OH (685 mg, 1.96 mmol, 0.7 M in *N*,*N*-dimethylformamide (DMF)) were introduced and the mixture was stirred at 70 °C for 30 min. The resin was washed with DMF and deprotection and coupling procedures were repeated with Asn(Trt)-OH (596.7 mg, 1.21 mmol, 0.7 M in DMF) to afford the resin-grafted tripeptide. The resin was washed with methanol and was treated with a TFA/H_2O/TIPS mixture (95/2.5/2.5, 7.55 mL) for 2 h at room temperature. Resin was filtrated and the filtrate was concentrated under reduced pressure. The residue was dissolved in acetone (10 mL) and precipitated with diethyl ether (50 mL) to afford the tripeptide **3** (222 mg, 82%), as a white solid.
^{1}H NMR (400 MHz, DMSO-*d*$_6$) δ 12.49 (s, 1H), 7.92 (dd, 2H, *J* = 23.0, 7.5 Hz), 7.68 (dd, 2H, *J* = 23.0, 7.5 Hz), 7.36 (ddd, 4H, *J* = 23.0, 15.0, 7.5 Hz), 7.25-7.07 (m, 1H), 6.92 (s, 1H), 4.61 (dd, 1H, *J* = 15.0, 7.5 Hz), 4.44 (d, 1H, *J* = 7.5 Hz), 4.31-4.15 (m, 2H), 4.07 (dd, 1H, *J* = 8.0, 6.2 Hz), 3.60-3.27 (m, 5H), 2.47-2.29 (m, 2H), 2.03 (ddd, 2H, *J* = 23.0, 15.0, 8.0 Hz), 1.87 (d, 2H, *J* = 4.1 Hz), 1.06-0.79 (m, 6H). HRMS (ESI) *m*/*z*: $[M+H]^+$ calcd for $C_{29}H_{35}N_4O_7$, 551.2500; found, 551.2494.

*5.2.3. Fmoc-Asn-Pro-Val-PAB-OH (**5**)*

To a solution of compound **3** (198 mg, 0.36 mmol) in dry DCM (2.5 mL) at 0 °C, under an argon atmosphere, were added DCC (111 mg, 0.54 mmol) and a catalytic amount of 4-dimethylaminopyridine (DMAP). The resulting mixture was stirred 1 h at 0 °C and 4-(((*tert*-butyldimethylsilyl)oxy)methyl)aniline (85 mg, 0.36 mmol) was added. The suspension was stirred overnight at room temperature, filtered on a celite pad, concentrated and purified by silica column chromatography using DCM with methanol (MeOH) gradient (0-8%) as eluent, to give intermediate **4** (167 mg, 60%) as a yellow oil (HRMS (ESI) *m*/*z*: $[M+Na]^+$ calcd for $C_{42}H_{55}N_5NaO_7Si$, 792.3769; found, 792.3767). To a solution of intermediate **4** (167 mg, 0.22 mmol) in absolute ethanol (2 mL) was added 20 µL of concentrated HCl (37% w/w). The resulting mixture turned red immediately and was stirred 2 h at room temperature. The solvent was then removed under reduced pressure, and the residue was finally purified by column chromatography

using DCM with MeOH gradient (0-10%) as eluent, to give compound **5** (132 mg, 92%, 55% over two steps) as an off-white powder.

^{1}H NMR (400 MHz, $CDCl_3$) δ 8.60 (s, 1H), 7.75 (d, 2H, J = 7.5 Hz), 7.59-7.47 (m, 5H), 7.42-7.28 (m, 4H), 7.20 (d, 2H, J = 7.5 Hz), 6.26-5.99 (m, 2H), 4.74-3.84 (m, 10H), 2.80-2.65 (m, 1H), 2.55-2.42 (m, 1H), 2.25-1.95 (m, 7H), 0.98 (dd, 6H, J = 14.0, 6.6 Hz). HRMS (ESI) *m/z*: $[M+H]^+$ calcd for $C_{36}H_{42}N_5O_7$, 656.3084; found, 656.3067.

*5.2.4. Fmoc-Asn-Pro-Val-PABC-PNP (**6**)*

A mixture of compound **5** (26.1 mg, 0.04 mmol), *para*-nitrophenyl chloroformate (16.1 mg, 0.08 mmol), and dry pyridine (8.0 µL, 0.10 mmol) in dry THF (2 mL), under an argon atmosphere, was stirred overnight at room temperature. The solvent was then removed under reduced pressure, and the residue was finally purified by column chromatography using DCM with MeOH gradient (0-8%) as eluent, to give intermediate **6** (31.4 mg, 96%) as an orange solid.

^{1}H NMR (300 MHz, $CDCl_3$) δ 8.95 (s, 1H), 8.29-8.17 (m, 2H), 7.74 (d, 2H, J = 6.0 Hz), 7.66 (d, 2H, J = 6.0 Hz), 7.56 (dd, 2H, J = 6.0, 3.0 Hz), 7.47-7.23 (m, 8H), 6.30 (s, 1H), 6.17 (d, 1H, J = 9.0 Hz), 5.62 (s, 1H), 5.21 (s, 2H), 4.90-4.72 (m, 1H), 4.70-4.50 (m, 1H), 4.45-4.10 (m, 4H), 3.78 (t, 2H, J = 6.0 Hz), 2.90-2,71 (m, 1H), 2.66-2.50 (m, 1H), 2.41-2.19 (m, 2H), 2.15-1.75 (m, 4H), 0.95 (dd, 6H, J = 21.0, 6.0 Hz). HRMS (ESI) *m/z*: $[M+Na]^+$ calcd for $C_{43}H_{44}N_6O_{11}Na$ 843.2966; found 843.2955.

*5.2.5. Fmoc-Asn-Pro-Val-PABC-MMAE (**7**)*

To a solution of compound **6** (25 mg, 0.03 mmol), hydroxybenzotriazole (HOBt) (14 mg, 0.10 mmol) and *N*,*N*'-diisopropylethylamine (DIPEA) (10.4 µL, 0.06 mmol) in dry DMF (1 mL), under an argon atmosphere, was added the trifluoroacetic salt of MMAE (15 mg, 0.02 mmol) in solution in dry DMF (1 mL). The resulting mixture was stirred overnight at room temperature and purified by semi-preparative HPLC (0.1% TFA, H_2O/ACN 80/20 method) to give intermediate **7** (20.4 mg, 48%) as a white solid.

^{1}H NMR (300 MHz, $CDCl_3$) δ 8.46 (bs, 1H), 7.90-7.65 (m, 4H), 7.63-7.22 (m, 2H), 7.49-7.27 (m, 11H), 6.70-3.69 (m, 16H), 3.64-1.45 (m, 39H), 1.35-1.10 (m, 4H), 1.08-0.42 (m, 29H). HRMS (ESI) *m/z*: $[M+H]^+$ calcd for $C_{76}H_{107}N_{10}O_{15}$, 1399.7917; found, 1399.7870.

*5.2.6. diSPhMC-Asn-Pro-Val-PABC-MMAE (**9**)*

To a solution of compound **7** (20 mg, 0.014 mmol) in dry DMF (800 µL) was added piperidine (200 µL). The resulting mixture was stirred 1 h at room temperature and purified by semi-preparative HPLC (0.1% TFA, H_2O/ACN 80/20 method) to give a mixture of compound **8** (6.0 mg estimated by NMR; HRMS (ESI) *m/z*: $[M+2H]^{2+}$ calcd for $C_{61}H_{98}N_{10}O_{13}$, 589.3658; found, 589.3655) inseparable from a TFA salt of piperidine. A mixture of compound **8** (6 mg, 0.005 mmol), intermediate **2** (2.8 mg, 0.005 mmol), HOBt (1.3 mg, 0.010 mmol) and DIPEA (1.74 µL, 0.011 mmol) in dry DMF (700 µL), under an argon atmosphere, was stirred overnight at room temperature. The resulting solution was then purified by semi-preparative HPLC (0.1% TFA, H_2O/ACN 80/20 method) to give linker-drug **9** (6.8 mg, 30% over two steps) as a yellow solid.

^{1}H NMR (300 MHz, DMSO-d_6) δ 9.93 (s, 1H), 8.43-6.86 (m, 26H), 5.37 (dd, 2H, J = 21.0, 6.0 Hz), 5.14-3.52 (m, 20H), 3.26-2.70 (m, 15H), 2.19-0.65 (m, 51H). HRMS (ESI) *m/z*: $[M+Na]^+$ calcd for $C_{83}H_{115}N_{11}NaO_{16}S_2$, 1608.7862; found, 1608.7944.

*5.3. Antibody conjugation, TTZ-MC-NPV-MMAE (**10**)*

Into three vials, were added trastuzumab (4.8 mg/mL, 500 µL) in BBS buffer (pH 8) and TCEP (97 µL, 6 eq, 1 mM in BBS buffer) and the reaction was incubated for 1.25 h at 37 °C. Linker **9** (97 µL, 6 eq, 1 mM in DMSO) was then added, and the reaction was incubated for 16 h at 4 °C under agitation (600 rpm). A second addition of TCEP (48 µL, 3 eq, 1 mM in BBS buffer) was performed and the reaction was incubated for 1.25 h at 37 °C. A second addition of the linker **9** (48 µL, 3 eq, 1 mM in DMSO) was performed, and the reaction was incubated for 22 h at 4 °C under agitation (600 rpm). The mixture was finally purified by size-exclusion chromatography (SEC) on a Superdex® 200 10/300 GL column (1.0 x 300 mm, 13 µM, molecular mass range 10, 000 - 600,000 Da) from Cytiva (GE Healthcare Life Sciences, 17-5174-01), connected to an Äkta purifier (Cytiva). The column was used at a rate of 0.8 mL/min with a UV detector at 280 nm. After the loading of TTZ-MC-NPV-MMAE, the column was eluted

with PBS for 0.2 column volume (cv), then with 0.3 cv of H_2O/ACN (7/3) + 0.2% TFA and finally with PBS (1 cv) to give TTZ-MC-NPV-MMAE (**10**) (4.8 mg, 67%).

5.4. ADC Analysis

5.4.1. Denaturing High-Resolution Mass Spectrometry

Denaturing high-resolution mass spectrometric analysis of ADCs were performed on a Bruker maXis mass spectrometer coupled to a Dionex Ultimate 3000 RSLC system. Prior to MS analysis, samples (ca. 5 µg) were desalted on a MassPREP desalting cartridge (2.1 × 10 mm, Waters) heated at 80 °C using 0.1% formic acid as solvent A and 0.1% formic acid in MeCN as solvent B at 500 µL/min. After 1 min, a linear gradient from 5 to 90% B in 1.5 min was applied; the first 1.5 min were diverted to waste. HRMS data were acquired in positive mode with ESI source over the m/z range from 900 up to 5000 at 1 Hz and processed using DataAnalysis 4.4 software (Bruker) and the MaxEnt algorithm for spectral deconvolution. Deconvolution was carried out in the range 20-180 kDa, with results recorded for full antibody (LHHL) and for fragments L, LH, HH, LHH (obtained from antibody dissociation during analysis). The average drug-to-antibody ratio (DAR) was calculated as an average of the percentage abundance of each present DAR species, with the quantities calculated by peak integration of the first glycosylation peak, following the corresponding formula:

$$DAR_{average} = \frac{DAR_{LHHL} + (DAR_{LHH} + DAR_{L}) + (2 * DAR_{L} + 2 * DAR_{H}) + 2 * DAR_{LH}}{4}$$

5.4.2. Hydrophobic Interaction Chromatography (HIC) analysis

TTZ-MC-NPV-MMAE (**10**) was diluted to 1 mg/mL in PBS pH 7.4 and filtered on a 0.22 µm PVDF membrane. Then 50 µg of the sample was injected on a MAbPac HIC-Butyl (4.6 × 100 mm, 5 µm) from Thermo Scientific, connected to a Waters Alliance (e2695) apparatus equipped with a photodiode array detector (2998) set for detection at 280 nm. Samples were run with a linear gradient from 100% buffer A (1.5 M ammonium sulfate, 50 mM sodium phosphate, 5% 2-propanol (v/v), pH 7.0) to 20% buffer B (50 mM sodium phosphate, 20% 2-propanol (v/v), pH 7.0) over 2 min and then to 85% buffer B over 30 min and held for 1 min at a flow rate of 1 mL/min. The column oven temperature was maintained at 25 °C. The drug-loaded species are resolved by

HIC based on the increasing hydrophobicity. The least hydrophobic and unconjugated form eluted first, while the most conjugated and hydrophobic form eluted last. The area percentage of each peak DAR_i represents the relative distribution of each particular drug-loaded ADC species. The weighted average DAR was then calculated using the percentage peak areas combined with their respective drug load numbers, according to the corresponding formula:

$$DAR_{average} = 0 * DAR_0 + 1 * DAR_1 + 2 * DAR_2 + 3 * DAR_3 + 4 * DAR_4 + 5 * DAR_5$$

5.4.3. Size-Exclusion Chromatography (SEC) Analysis

ADCs were diluted to 1 mg/mL with PBS pH 7.4 and filtered on a 0.22 µm PVDF membrane. A sample of 40 µg was injected on an AdvanceBio SEC (7.8 × 300 mm, 2.7 µm) from Agilent Technologies, connected to a Waters Alliance (e2695) apparatus equipped with a photodiode array detector (2998) set for detection at 280 nm. Samples were run with an isocratic gradient (1 mM potassium phosphate monobasic, 155 mM sodium chloride, 3 mM sodium phosphate dibasic, 3 mM sodium azide, pH 7.0) over 24 min at a flow rate of 1 mL/min. The column oven temperature was maintained at 25 °C.

5.5. Biology

5.5.1. ELISA assays

HER2 recombinant protein (Sino Biologicals, Beijing, P. R. China) was coated in a 96-well plates at 1 µg.mL^{-1} in PBS and incubated overnight at 4 °C. The wells were then saturated with 3% BSA-PBS for 1 h at 37 °C, and washed with PBS prior to incubation with PBS (negative control), ADCs or trastuzumab (Ontruzant®, MSD laboratory, France) from 0.001 to 300 µM during 1 h at 37 °C. Wells were then washed with PBS-Tween 20 (0.05%) and incubated with 100 µL of protein-L-peroxydase (ThermoScientific, Pierce®, Massachusetts, USA) at 1.25 µg.mL^{-1} for 1 h at 37 °C, and 100 µL of 3,3',5,5'-tetramethylbenzidine substrate (TMB) (Sigma, St Louis, USA) were added in each well. Enzymatic reactions were stopped with the addition of 50 µL of 1 M H_2SO_4 and the absorbance was measured at 450 nm, using an absorbance microplate reader (Bio-Tek® instruments, Inc., Vermont, USA).

5.5.2. Enzymatic Cleavage Assays

HNE (#324681, Sigma-Aldrich) was diluted to 50 µg/mL in 0.1 M Tris-HCl pH 8.0. The cleavage of NPV linker was first realized. The reactivity of the diphenylthiomaleimide scaffold of linker **9** prevented its use in this biochemical cleavage test; the NPV-containing intermediate **8** was thus evaluated. The enzyme substrate MeO-Suc-Ala-Ala-Pro-Val-pNA (#M4765, Sigma-Aldrich) was used as positive control to validate HNE activity. A solution of compound **8** or MeO-Suc-Ala-Ala-Pro-Val-pNA (9 µL of a 2 mM solution in DMSO), Tris-HCl 0.1 M pH 8.0 (49 µL) and HNE (2 µL), for conditions with HNE, or Tris-HCl 0.1 M pH 8.0 (2 µL), for conditions without HNE, was incubated for 24 h at 37 °C. Samples were then analyzed by HPLC with a UV detection at 254 nm (for MeO-Suc-Ala-Ala-Pro-Val-pNA) or at 215 nm for the MMAE-containing compound **8**. Elution was performed with 0.1% TFA in water (solvent A), and 0.1% TFA in MeCN (solvent B), with a gradient from 20 to 100% of B over 32 min and then 100% of B for 6 min at 17.1 mL/min.

For the cleavage of the whole ADC **10** experiment, a 6 µM solution in PBS (pH 7.4) of conjugate **10** was incubated at 37 °C for 2 h with HNE (0.15 µM) or without HNE. Samples were analyzed by denaturing mass spectrometry (*cf.* 5.4.1).

5.5.3. Confocal Fluorescence Microscopy

Protein L coupled with phycoerythrin (ppL-PE, Sinobiological, *Beijing, China*) was used as an intracellular tracer. Protein L was obtained from *Peptostreptococcus magnus*. This protein possesses a high affinity for kappa light chain of anti-HER2-like antibodies. Briefly, 30,000 SK-BR-3 and MDA-MB-231 cells were seeded 48 h on p-D-lysine coated glass slides. ADCs were then incubated 30 minutes with ppL-PE in a 1:2 ratio at 37 °C, and 10 nmol/L of ADC-ppL-PE complexes were incubated on cells for 48 h. Cells were washed three times with cold PBS. Finally, glass slides were assembled on the reverse side with a mounting medium, Fluoromount-G (Thermofisher, Waltham MA, USA). Observations were carried out on a fluorescence confocal microscope (Leica SP8 Confocal Microscope, Leica Microsystèmes, Nanterre, France) with a x63 objective lens and a white light laser (Leica). Images were analyzed by Leica Application Suite X software.

5.5.4. Flow Cytometry Studies

Briefly, 50,000 SK-BR-3 and MDA-MB-231 cells were seeded 24 h on 24-well plates. ADCs were then incubated 30 minutes with ppL-PE (1:2 ratio) at 37 °C, and 10 nmol/L of ADC-ppL-PE complexes were incubated on cells with or without elastase enzyme for 48 h. Cells were then washed three times with cold PBS, and transferred on 96 round bottom wells plates in a PBS, BSA 1% and EDTA 2 mM solution. Finally, cells were analyzed by a MACSQuant 10 flow cytometer (Miltenyi Biotec) with an excitation laser at 488 nm (filter 565-605 nm) to detect PE fluorescence.

5.5.5. Cell Cultures and Reagents

MDA-MB-231 human breast carcinoma cells were obtained from the American Type Culture Collection (LGC Promochem, Molsheim, France). The cells were cultured in Dulbecco's Modified Eagle Medium (DMEM), with 10% fetal bovine serum (FBS, Gibco®), glucose, L-glutamine, and 1% Penicillin-Streptomycin solution (10,000 U/mL, Gibco®) at 37 °C and 5% CO_2. SK-BR-3 cell lines were obtained from Cell Lines Service (CLS Eppelheim, Germany). SK-BR-3 cells were maintained in DMEM supplemented with 10% FBS and 1% Penicillin-Streptomycin solution, in humidified atmosphere at 37 °C with 5% CO_2.

5.5.6. Cell Proliferation Assays

Cell viability and proliferation were studied, using a luminescent test based on quantification of ATP, using the CellTiter-Glo cell proliferation assay (Promega Wiscousin, USA). Briefly, 6.000 SK-BR-3 cells or 3.000 MDA-MB-231 cells were incubated in 100 µL of medium in 96-well plates for 24 h and then treated with concentrations ranging from 0.001 nM to 1000 nM of tested compounds. For the conditions with elastase, 50 µL of medium were removed and HNE (#324681, Sigma-Aldrich) was added at a final concentration of 50 nM. Cells were incubated with 100 µL of each compound at 37 °C with 5% CO_2 for 5 days. A H_2O_2 solution at 10 mM was used as positive control. A HNE solution at 50 nM and culture medium alone were tested as negative controls. MMAE (100 nM, stock solution at 2 µM in PBS) and trastuzumab (100 nM, stock solution at 26 µM in PBS) were used as reference. Cells were incubated with 100 µL of each solution at 37 °C with 5% CO_2 for 5 days. Cell

viability was then determined using CellTiter-Glo reagent (Promega, Wiscousin, USA). Briefly, 100 µL of medium were removed and 100 µL of CellTiter-Glo reagent were added to each well. The plates were shaken 2 min and then incubated at room temperature for 10 min. The luminescence values were measured with a gain at 135, with an acquisition at 0.5 s, using an absorbance microplate reader (Bio-Tek® instruments, Inc., Vermont, USA). When a dose-dependent activity was observed, 50% inhibitory concentration (IC_{50}) were calculated using Graphpad PRISM 7 software (n = 4 in quadruplicate).

Acknowledgments

This work was supported by the French National Research Agency under the program "Investissements d'avenir" Grant Agreement LabEx MAbImprove (ANR-10-LABX-53-01), Tours University, La Ligue contre le cancer (comities 18, 35, 36, 37, 41, 44, 53, 72, 79, 85), the Centre-Val de Loire Region (projects ARD 2020 Biomédicament: MabCHEM and BIOS, and project APR IR 2017) and FEDER (Fonds européen de développement régional). S. Huvelle and S. Henrion thank Centre-Val de Loire Region for their postdoctoral fellowships. I. Ait Mohamed Amar thanks Centre-Val de Loire Region for her PhD fellowship. The authors thank the « *Plateforme Scientifique et Technique Analyses des Systèmes Biologiques* » (PST-ASB), Tours (France), for NMR spectrometry. We thank Eloi Haudebourg, Vincent Caulier, and Nicolas Albrecht from the team IMT GICC EA7501 for mass analysis.

References

[1] N. Joubert, A. Beck, C. Dumontet, C. Denevault-Sabourin, Antibody-Drug Conjugates : The Last Decade, Pharmaceuticals. 13 (2020) 235. doi:10.3390/ph13090245.

[2] A. Beck, L. Goetsch, C. Dumontet, N. Corvaïa, Strategies and challenges for the next generation of antibody-drug conjugates, Nat. Rev. Drug Discov. 16 (2017) 315–337. doi:10.1038/nrd.2016.268.

[3] H. Merten, F. Brandl, A. Plückthun, U. Zangemeister-Wittke, Antibody-Drug

607 Conjugates for Tumor Targeting - Novel Conjugation Chemistries and the
608 Promise of non-IgG Binding Proteins, Bioconjug. Chem. 26 (2015) 2176–2185.
609 doi:10.1021/acs.bioconjchem.5b00260.
610 [4] R.V.J. Chari, M.L. Miller, W.C. Widdison, Antibody-drug conjugates: An
611 emerging concept in cancer therapy, Angew. Chemie - Int. Ed. 53 (2014) 3796–
612 3827. doi:10.1002/anie.201307628.
613 [5] H. Bouchard, C. Viskov, C. Garcia-Echeverria, Antibody-drug conjugates - A
614 new wave of cancer drugs, Bioorganic Med. Chem. Lett. 24 (2014) 5357–5363.
615 doi:10.1016/j.bmcl.2014.10.021.
616 [6] U. Hafeez, S. Parakh, H.K. Gan, A.M. Scott, Antibody-drug conjugates for
617 cancer therapy, Molecules. 25 (2020) 4764. doi:10.3390/molecules25204764.
618 [7] C. Denevault-Sabourin, F. Bryden, M.-C. Viaud-Massuard, N. Joubert,
619 Antibody-drug conjugates: Empowering antibodies for the fight against cancer,
620 Successful Drug Discovery, 4 (2019) 55–82. doi:10.1002/9783527814695.ch3.
621 [8] H.K. Erickson, P.U. Park, W.C. Widdison, Y. V. Kovtun, L.M. Garrett, K.
622 Hoffman, R.J. Lutz, V.S. Goldmacher, W.A. Blättler, Antibody-maytansinoid
623 conjugates are activated in targeted cancer cells by lysosomal degradation and
624 linker-dependent intracellular processing, Cancer Res. 66 (2006) 4426–4433.
625 doi:10.1158/0008-5472.CAN-05-4489.
626 [9] Y. V. Kovtun, C.A. Audette, Y. Ye, H. Xie, M.F. Ruberti, S.J. Phinney, B.A.
627 Leece, T. Chittenden, W.A. Blättler, V.S. Goldmacher, Antibody-drug conjugates
628 designed to eradicate tumors with homogeneous and heterogeneous expression of
629 the target antigen, Cancer Res. 66 (2006) 3214–3221. doi:10.1158/0008-
630 5472.CAN-05-3973.
631 [10] N. Joubert, C. Denevault-Sabourin, F. Bryden, M.-C. Viaud-Massuard, Towards
632 antibody-drug conjugates and prodrug strategies with extracellular stimuli-
633 responsive drug delivery in the tumor microenvironment for cancer therapy, Eur.
634 J. Med. Chem. 142 (2017) 393–415. doi:10.1016/j.ejmech.2017.08.049.
635 [11] M. Barok, H. Joensuu, J. Isola, Trastuzumab emtansine: mechanisms of action
636 and drug resistance, Breast Cancer Res. 16 (2014) 3378. doi:10.1186/bcr3621.
637 [12] G. Li, J. Guo, B.Q. Shen, D.B. Yadav, M.X. Sliwkowski, L.M. Crocker, J.A.
638 Lacap, G.D.L. Phillips, Mechanisms of acquired resistance to trastuzumab

emtansine in breast cancer cells, Mol. Cancer Ther. 17 (2018) 1441–1453. doi:10.1158/1535-7163.MCT-17-0296.

[13] F.W. Hunter, H.R. Barker, B. Lipert, F. Rothé, G. Gebhart, M.J. Piccart-Gebhart, C. Sotiriou, S.M.F. Jamieson, Mechanisms of resistance to trastuzumab emtansine (T-DM1) in HER2-positive breast cancer, Br. J. Cancer. 122 (2020) 603–612. doi:10.1038/s41416-019-0635-y.

[14] C. Ríos-Luci, S. García-Alonso, E. Díaz-Rodríguez, M. Nadal-Serrano, J. Arribas, A. Ocaña, A. Pandiella, Resistance to the antibody–drug conjugate T-DM1 is based in a reduction in lysosomal proteolytic activity, Cancer Res. 77 (2017) 4639–4651. doi:10.1158/0008-5472.CAN-16-3127.

[15] K.J. Hamblett, A.P. Jacob, J.L. Gurgel, M.E. Tometsko, B.M. Rock, S.K. Patel, R.R. Milburn, S. Siu, S.P. Ragan, D.A. Rock, C.J. Borths, J.W.O. Neill, W.S. Chang, M.F. Weidner, M.M. Bio, K.C. Quon, W.C. Fanslow, SLC46A3 Is Required to Transport Catabolites of Noncleavable Antibody Maytansine Conjugates from the Lysosome to the Cytoplasm, Cancer Res. 75 (2015) 5329–5340. doi:10.1158/0008-5472.CAN-15-1610.

[16] J. Sauveur, E.-L. Matera, K. Chettab, P. Valet, J. Guitton, A. Savina, C. Dumontet, Esophageal cancer cells resistant to T-DM1 display alterations in cell adhesion and the prostaglandin pathway, Oncotarget. 9 (2018) 21141–21155. doi:10.18632/oncotarget.24975.

[17] A.H. Staudacher, M.P. Brown, Antibody drug conjugates and bystander killing: is antigen-dependent internalisation required, Br. J. Cancer. 117 (2017) 1736–1742. doi:10.1038/bjc.2017.367.

[18] J.F. DiJoseph, M.M. Dougher, D.C. Armellino, L. Kalyandrug, A. Kunz, E.R. Boghaert, P.R. Hamann, N.K. Damle, CD20-specific antibody-targeted chemotherapy of non-Hodgkin B-cell lymphoma using calicheamicin-conjugated rituximab, Cancer Immunol. Immunother. 56 (2007) 1107–1117. doi:10.1007/s00262-006-0260-5.

[19] R.M. Sharkey, H. Karacay, S. V. Govindan, D.M. Goldenberg, Combination radioimmunotherapy and chemoimmunotherapy involving different or the same targets improves therapy of human pancreatic carcinoma xenograft models, Mol. Cancer Ther. 10 (2011) 1072–1081. doi:10.1158/1535-7163.MCT-11-0115.

671 [20] S. V. Govindan, T.M. Cardillo, S.J. Moon, H.J. Hansen, D.M. Goldenberg,
672 CEACAM5-targeted therapy of human colonic and pancreatic cancer xenografts
673 with potent labetuzumab-SN-38 immunoconjugates, Clin. Cancer Res. 15 (2009)
674 6052–6061. doi:10.1158/1078-0432.CCR-09-0586.
675 [21] G.J.L. Bernardes, G. Casi, S. Trüssel, I. Hartmann, K. Schwager, J.
676 Scheuermann, D. Neri, A traceless vascular-targeting antibody-drug conjugate
677 for cancer therapy, Angew. Chemie - Int. Ed. 51 (2012) 941–944.
678 doi:10.1002/anie.201106527.
679 [22] M. Steiner, I. Hartmann, E. Perrino, G. Casi, S. Brighton, I. Jelesarov, G.J.L.
680 Bernardes, D. Neri, Spacer length shapes drug release and therapeutic efficacy of
681 traceless disulfide-linked ADCs targeting the tumor neovasculature, Chem. Sci. 4
682 (2013) 297–302. doi:10.1039/c2sc21107f.
683 [23] R. Gébleux, M. Stringhini, R. Casanova, A. Soltermann, D. Neri, Non-
684 internalizing antibody-drug conjugates display potent anti-cancer activity upon
685 proteolytic release of monomethyl auristatin E in the subendothelial extracellular
686 matrix, Int. J. Cancer. 140 (2017) 1670–1679. doi:10.1002/ijc.30569.
687 [24] A.G. Poison, J. Calemine-Fenaux, P. Chan, W. Chang, E. Christensen, S. Clark,
688 F.J. De Sauvage, D. Eaton, K. Elkins, J. Michael Elliott, G. Frantz, R.N. Fuji, A.
689 Gray, K. Harden, G.S. Ingle, N.M. Kljavin, H. Koeppen, C. Nelson, S. Prabhu,
690 H. Raab, S. Ross, J.P. Stephan, S.J. Scales, S.D. Spencer, R. Vandlen, B. Wranik,
691 S.F. Yu, B. Zheng, A. Ebens, Antibody-drug conjugates for the treatment of non-
692 Hodgkin's lymphoma: Target and linker-drug selection, Cancer Res. 69 (2009)
693 2358–2364. doi:10.1158/0008-5472.CAN-08-2250.
694 [25] C. Szot, D.S. Dimitrov, B.S. Croix, C. Szot, S. Saha, X.M. Zhang, Z. Zhu, M.B.
695 Hilton, K. Morris, S. Seaman, J.M. Dunleavey, K. Hsu, G. Yu, H. Morris, D.A.
696 Swing, D.C. Haines, Y. Wang, J. Hwang, Y. Feng, D. Welsch, G. Decrescenzo,
697 A. Chaudhary, E. Zudaire, D.S. Dimitrov, B.S. Croix, Tumor stroma-targeted
698 antibody-drug conjugate triggers localized anticancer drug release, 128 (2018)
699 2927–2943. doi: 10.1172/JCI120481.
700 [26] S.O. Doronina, B.E. Toki, M.Y. Torgov, B.A. Mendelsohn, C.G. Cerveny, D.F.
701 Chace, R.L. DeBlanc, R.P. Gearing, T.D. Bovee, C.B. Siegall, J.A. Francisco,
702 A.F. Wahl, D.L. Meyer, P.D. Senter, Development of potent monoclonal

703 antibody auristatin conjugates for cancer therapy, Nat. Biotechnol. 21 (2003)
704 778–784. doi:10.1038/nbt832.
705 [27] G.M. Dubowchik, R.A. Firestone, L. Padilla, D. Willner, S.J. Hofstead, K.
706 Mosure, J.O. Knipe, S.J. Lasch, P.A. Trail, Cathepsin B-labile dipeptide linkers
707 for lysosomal release of doxorubicin from internalizing immunoconjugates:
708 Model studies of enzymatic drug release and antigen-specific in vitro anticancer
709 activity, Bioconjug. Chem. 13 (2002) 855–869. doi:10.1021/bc025536j.
710 [28] H.G. Lerchen, J. Baumgarten, A. Schoop, M. Albers, Enzyme-activated
711 cytostatic conjugates with integrin ligands. PCT/WO 072151, 2002.
712 [29] I. Lerman, S.R. Hammes, Neutrophil elastase in the tumor microenvironment,
713 Steroids. 133 (2018) 96–101. doi:10.1016/j.steroids.2017.11.006.
714 [30] A. Raposo Moreira Dias, A. Pina, A. Dean, H.G. Lerchen, M. Caruso, F.
715 Gasparri, I. Fraietta, S. Troiani, D. Arosio, L. Belvisi, L. Pignataro, A. Dal Corso,
716 C. Gennari, Neutrophil Elastase Promotes Linker Cleavage and Paclitaxel
717 Release from an Integrin-Targeted Conjugate, Chem. - A Eur. J. 25 (2019) 1696–
718 1700. doi:10.1002/chem.201805447.
719 [31] N. Aubrey, E. Allard-Vannier, C. Martin, F. Bryden, S. Letast, C. Colas, Z.
720 Lakhrif, N. Collinet, I. Dimier-Poisson, I. Chourpa, M.C. Viaud-Massuard, N.
721 Joubert, Site-Specific Conjugation of Auristatins onto Engineered scFv Using
722 Second Generation Maleimide to Target HER2-positive Breast Cancer in Vitro,
723 Bioconjug. Chem. 29 (2018) 3516–3521. doi:10.1021/acs.bioconjchem.8b00668.
724 [32] F. Bryden, C. Martin, S. Letast, E. Lles, I. Viéitez-Villemin, A. Rousseau, C.
725 Colas, M. Brachet-Botineau, E. Allard-Vannier, C. Larbouret, M.C. Viaud-
726 Massuard, N. Joubert, Impact of cathepsin B-sensitive triggers and hydrophilic
727 linkers on in vitro efficacy of novel site-specific antibody-drug conjugates, Org.
728 Biomol. Chem. 16 (2018) 1882–1889. doi:10.1039/c7ob02780j.
729 [33] N. Joubert, C. Martin, G. Brachet, C. Colas, E. Allard-Vannier, C. Kizlik-
730 Masson, C. Esnault, R. Respaud, C. Denevault-Sabourin, I. Chourpa, V.
731 Gouilleux-Gruart, M.C. Viaud-Massuard, In vitro characterization and stability
732 profiles of antibody–fluorophore conjugates derived from interchain cysteine
733 cross-linking or lysine bioconjugation, Pharmaceuticals. 12 (2019) 176.
734 doi:10.3390/ph12040176.

[34] V. Corvaglia, M. Amar, V. Garambois, C. Gongora, M. Del Rio, C. Denevault-sabourin, N. Joubert, I. Huc, P. Pourquier, Internalization of Foldamer-Based DNA Mimics through a Site-Specific Antibody Conjugate to Target HER2-Positive Cancer Cells, Pharmaceuticals. 14 (2021) 624.

[35] F.F. Schumacher, J.P.M. Nunes, A. Maruani, V. Chudasama, M.E.B. Smith, K.A. Chester, J.R. Baker, S. Caddick, Next generation maleimides enable the controlled assembly of antibody-drug conjugates via native disulfide bond bridging, Org. Biomol. Chem. 12 (2014) 7261. doi:10.1039/C4OB01550A.

[36] J.P.M. Nunes, M. Morais, V. Vassileva, E. Robinson, V.S. Rajkumar, M.E.B. Smith, R.B. Pedley, S. Caddick, J.R. Baker, V. Chudasama, Functional native disulfide bridging enables delivery of a potent, stable and targeted antibody-drug conjugate (ADC), Chem. Commun. 51 (2015) 10624–10627. doi:10.1039/C5CC03557K.

[37] G. Badescu, P. Bryant, M. Bird, K. Henseleit, J. Swierkosz, V. Parekh, R. Tommasi, E. Pawlisz, K. Jurlewicz, M. Farys, N. Camper, X. Sheng, M. Fisher, R. Grygorash, A. Kyle, A. Abhilash, M. Frigerio, J. Edwards, A. Godwin, Bridging disulfides for stable and defined antibody drug conjugates, Bioconjug. Chem. 25 (2014) 1124–1136. doi:10.1021/bc500148x.

[38] C.R. Behrens, E.H. Ha, L.L. Chinn, S. Bowers, G. Probst, M. Fitch-Bruhns, J. Monteon, A. Valdiosera, A. Bermudez, S. Liao-Chan, T. Wong, J. Melnick, J.W. Theunissen, M.R. Flory, D. Houser, K. Venstrom, Z. Levashova, P. Sauer, T.S. Migone, E.H. Van Der Horst, R.L. Halcomb, D.Y. Jackson, Antibody-Drug Conjugates (ADCs) Derived from Interchain Cysteine Cross-Linking Demonstrate Improved Homogeneity and Other Pharmacological Properties over Conventional Heterogeneous ADCs, Mol. Pharm. 12 (2015) 3986–3998. doi:10.1021/acs.molpharmaceut.5b00432.

[39] K.J. Hamblett, P.D. Senter, D.F. Chace, M.M.C. Sun, J. Lenox, C.G. Cerveny, K.M. Kissler, S.X. Bernhardt, A.K. Kopcha, R.F. Zabinski, D.L. Meyer, J.A. Francisco, Effects of drug loading on the antitumor activity of a monoclonal antibody drug conjugate, Clin. Cancer Res. 10 (2004) 7063–7070. doi:10.1158/1078-0432.CCR-04-0789.

[40] M.M.C. Sun, K.S. Beam, C.G. Cerveny, K.J. Hamblett, R.S. Blackmore, M.Y.

767 Torgov, F.G.M. Handley, N.C. Ihle, P.D. Senter, S.C. Alley, Reduction-
768 alkylation strategies for the modification of specific monoclonal antibody
769 bisulfides, Bioconjug. Chem. 16 (2005) 1282–1290. doi:10.1021/bc050201y.
770 [41] S.P.M. Crouch, R. Kozlowski, K.J. Slater, J. Fletcher, The use of ATP
771 bioluminescence as a measure of cell proliferation and cytotoxicity, 160 (1993)
772 81–88.
773 [42] D. Hanahan, R.A. Weinberg, Hallmarks of cancer: The next generation, Cell. 144
774 (2011) 646–674. doi:10.1016/j.cell.2011.02.013.
775 [43] K.M. Haynes, N. Abdali, V. Jhawar, H.I. Zgurskaya, J.M. Parks, A.T. Green, J.
776 Baudry, V. V. Rybenkov, J.C. Smith, J.K. Walker, Identification and Structure-
777 Activity Relationships of Novel Compounds that Potentiate the Activities of
778 Antibiotics in Escherichia coli, J. Med. Chem. 60 (2017) 6205–6219.
779 doi:10.1021/acs.jmedchem.7b00453.
780
781

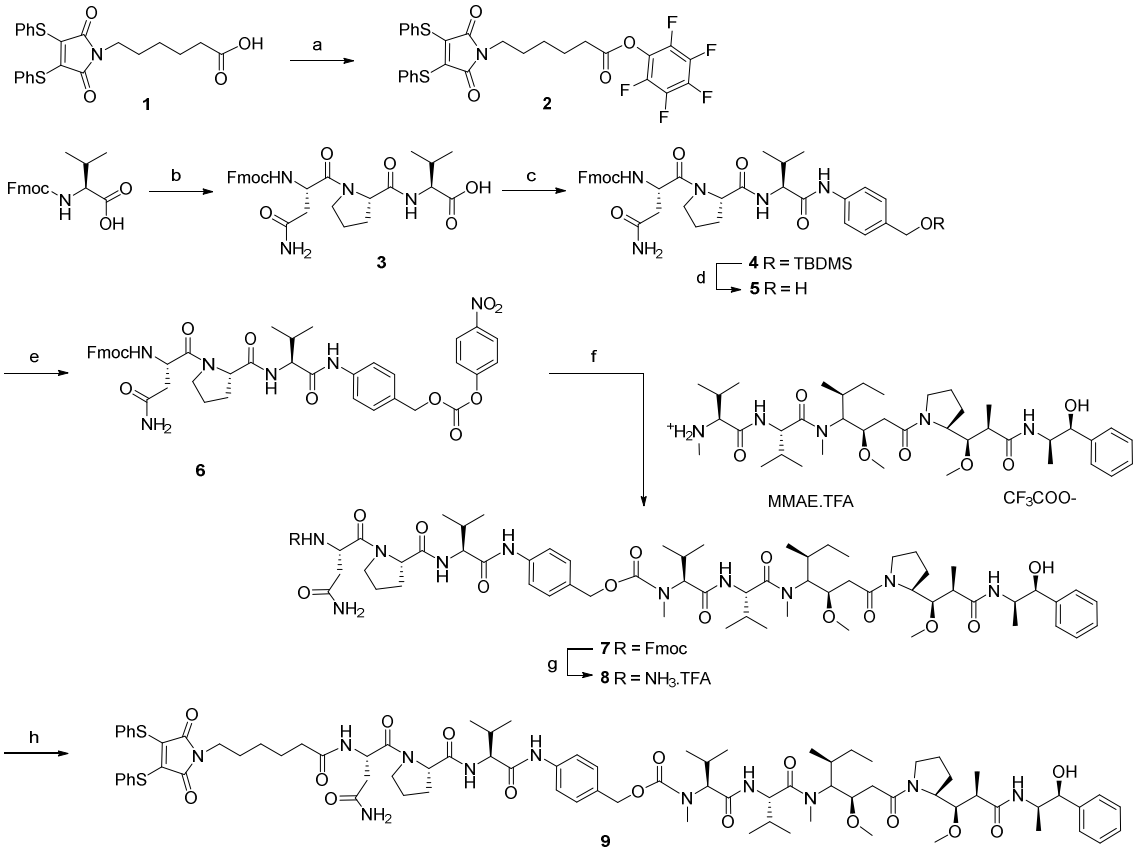

Scheme 1. Reagents and conditions: (a) **1** (1 eq), pentafluorophenol (1 eq), *N*,*N*'-dicyclohexylcarbodiimide (DCC) (1 eq), THF, 0 °C, and then rt, overnight, 91%; (b) 1) Fmoc-Pro-OH (4 eq), diisopropylcarbodiimide (DIC) (4 eq), Oxyma (4 eq), DMF, *N*-methyl-2-pyrrolidone, 70 °C, 30 min, 2) Fmoc-Asn(Trt)-OH (1.5 eq), DIC (4 eq), Oxyma (4 eq), DMF, *N*-methyl-2-pyrrolidone, 70 °C, 30 min, 3) TFA/H_2O/TIPS, MeOH, rt, 2 h, 82%; (c) 1) DCC (1.5 eq), 4-dimethylaminopyridine (cat.), DCM, 0 °C, 1 h, 2) 4-(((*tert*-butyldimethylsilyl)oxy)methyl)aniline (1 eq), rt, overnight, 60%; (d) HCl (37%), EtOH, rt, 2 h, 92%; (e) *para*-nitrophenyl chloroformate (2 eq), pyridine (2.5 eq), THF, rt, overnight, 96%; (f) MMAE TFA salt (0.67 eq), hydroxybenzotriazole (HOBt) (3.3 eq), *N*,*N*'-diisopropylethylamine (DIPEA) (2 eq), DMF, rt, overnight, 48%; (g) Piperidine (20%), DMF, rt, 1 h, then (h) **2** (1 eq), HOBt (2 eq), DIPEA (2.2 eq), DMF, rt, overnight, 30% over two steps.

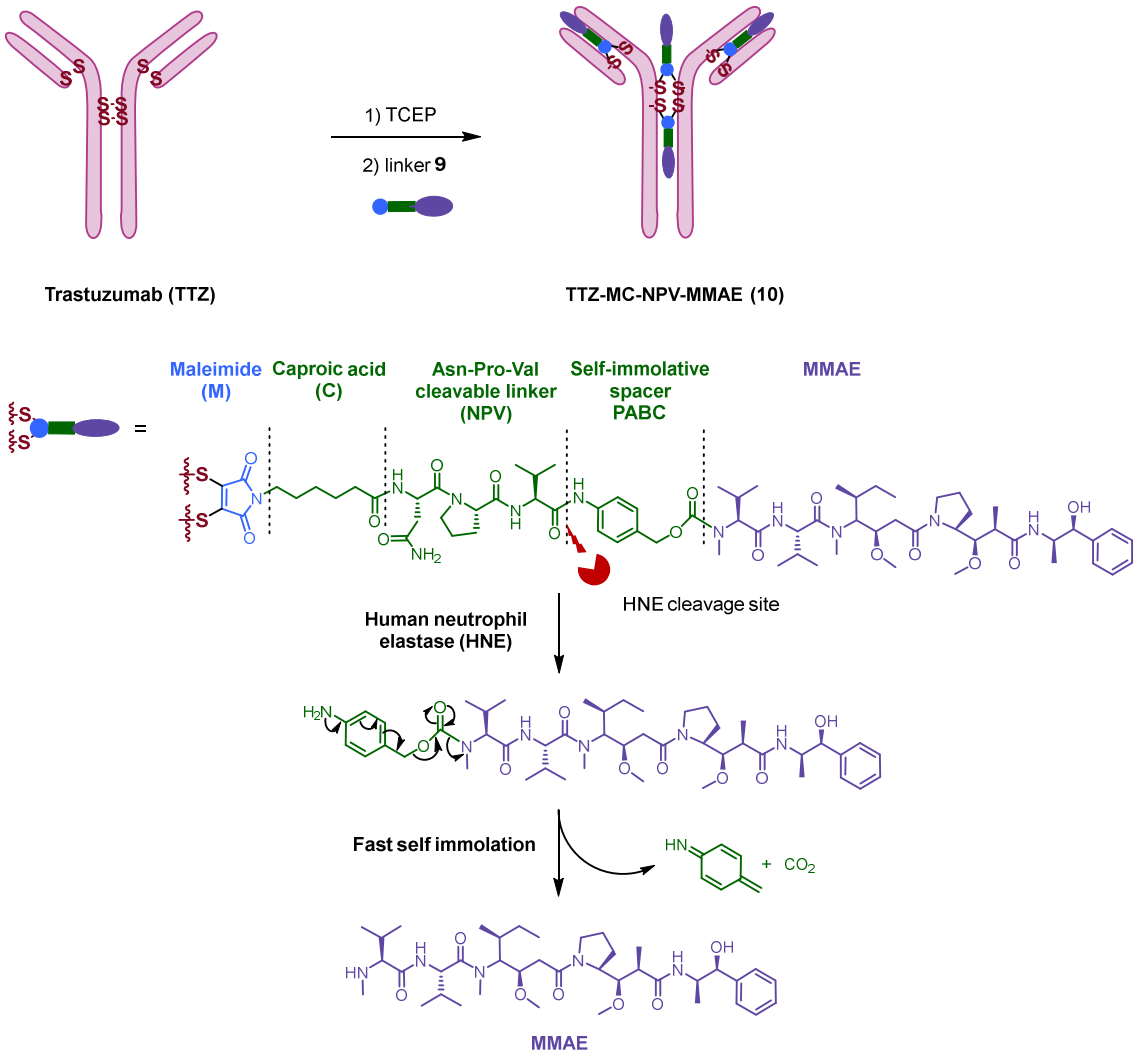

798

799 **Fig. 1.** Bioconjugation process, structure, and mechanism of MMAE release of the

800 TTZ-MC-NPV-MMAE (**10**).

801

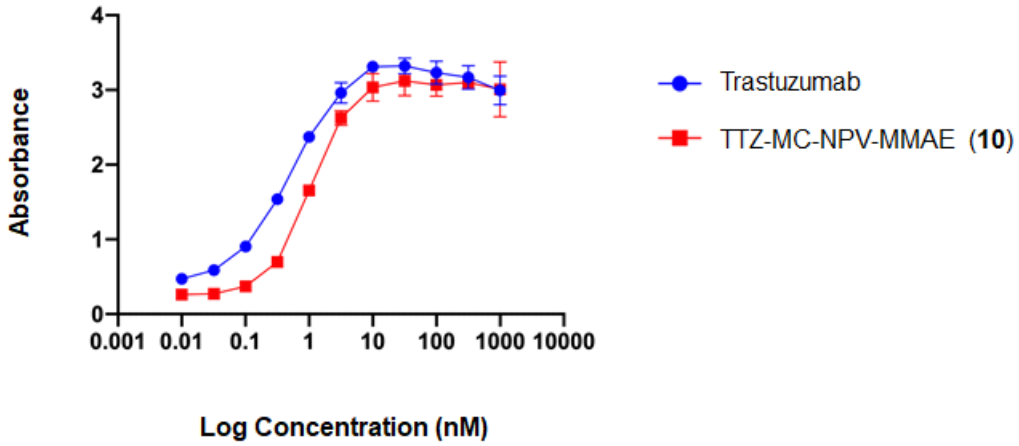

802
803

804 **Fig. 2.** HER2 binding affinities of TTZ-MC-NPV-MMAE (**10**) (red curve) in
805 comparison to trastuzumab (blue curve) determined by ELISA.

806
807

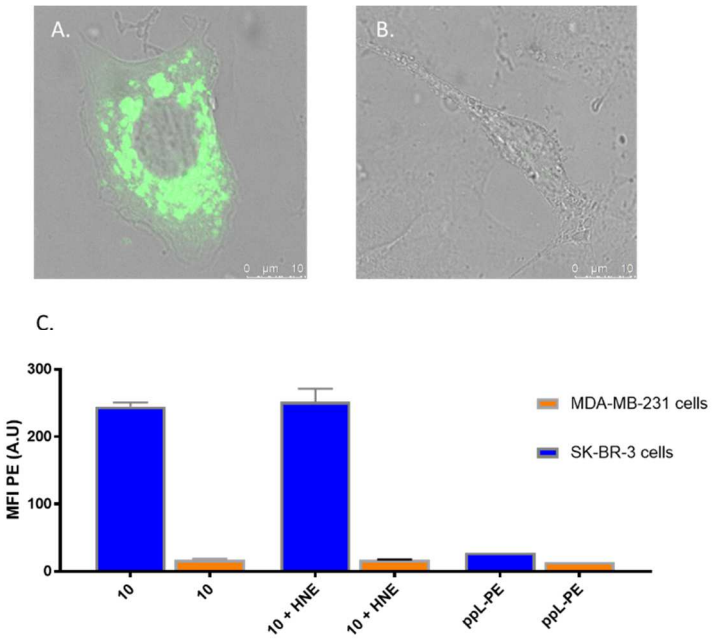

808

809 **Fig. 3.** Confocal microscopy images of SK-BR-3 (HER2+) (A) and MDA-MB-231
810 (HER2-) (B) cell lines after exposure to TTZ-MC-NPV-MMAE (**10**) for 48 h. (C)
811 Internalization of ADC **10** after complexation with ppL-PE in SK-BR-3 and MDA-MB-
812 231 cell lines, as analyzed by flow cytometry (exposure time = 48 h).

813

814

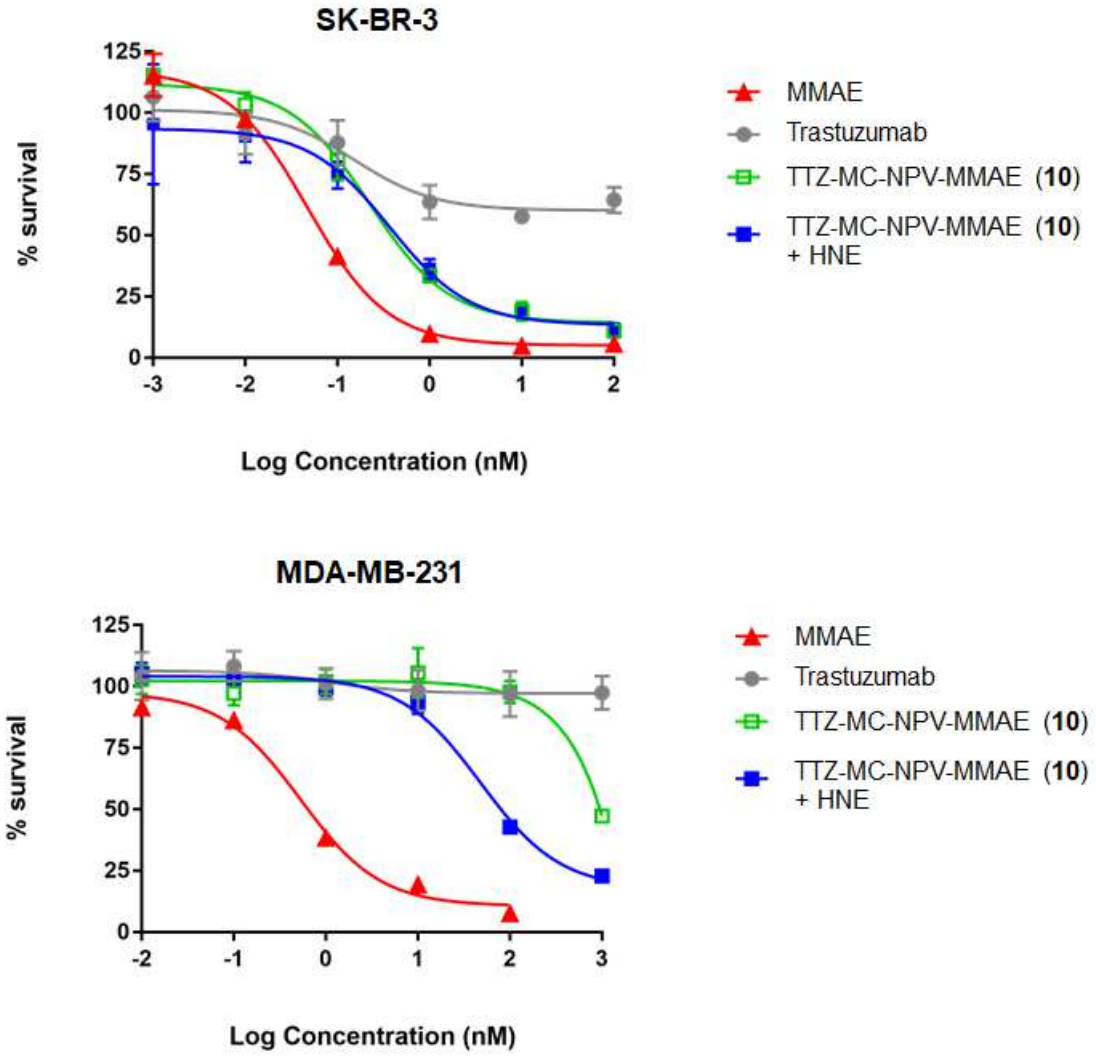

Fig. 4. *In vitro* cytotoxic activity of TTZ-MC-NPV-MMAE (**10**) in comparison to trastuzumab and free MMAE on SK-BR-3 and MDA-MB-231 cancer cell lines.

Table 1

Cell-based assays of TTZ-MC-NPV-MMAE (**10**) with or without HNE.

		IC_{50} (nM)[a]	
Entry	Compd	SK-BR-3 (HER2+)[b]	MDA-MB-231 (HER2-)[b]
1	ADC **10**	0.23 ± 0.08	› 1000
2	ADC **10** + HNE[c]	0.36 ± 0.13	47.5 ± 7.9
3	Trastuzumab	> 1000	› 1000
4	MMAE	0.05 ± 0.01	0.53 ± 0.06

[a] IC_{50} were calculated from dose-response curves. Each compound concentration was tested in quadruplicate.

[b] Cells were treated for 5 days, with concentrations ranging from 0.01 to 1000 nM for MDA-MB-231 cells and from 0.001 to 100 nM for SK-BR-3 cells. Cell viability was determined by quantification of ATP, using the CellTiter-Glo cell proliferation assay, and IC_{50} values were calculated using Graphpad PRISM 7 software (n = 4 in quadruplicate).

[c] HNE enzyme was added at a final concentration of 50 nM, concentration at which HNE had a negligible effect on cell viability alone.

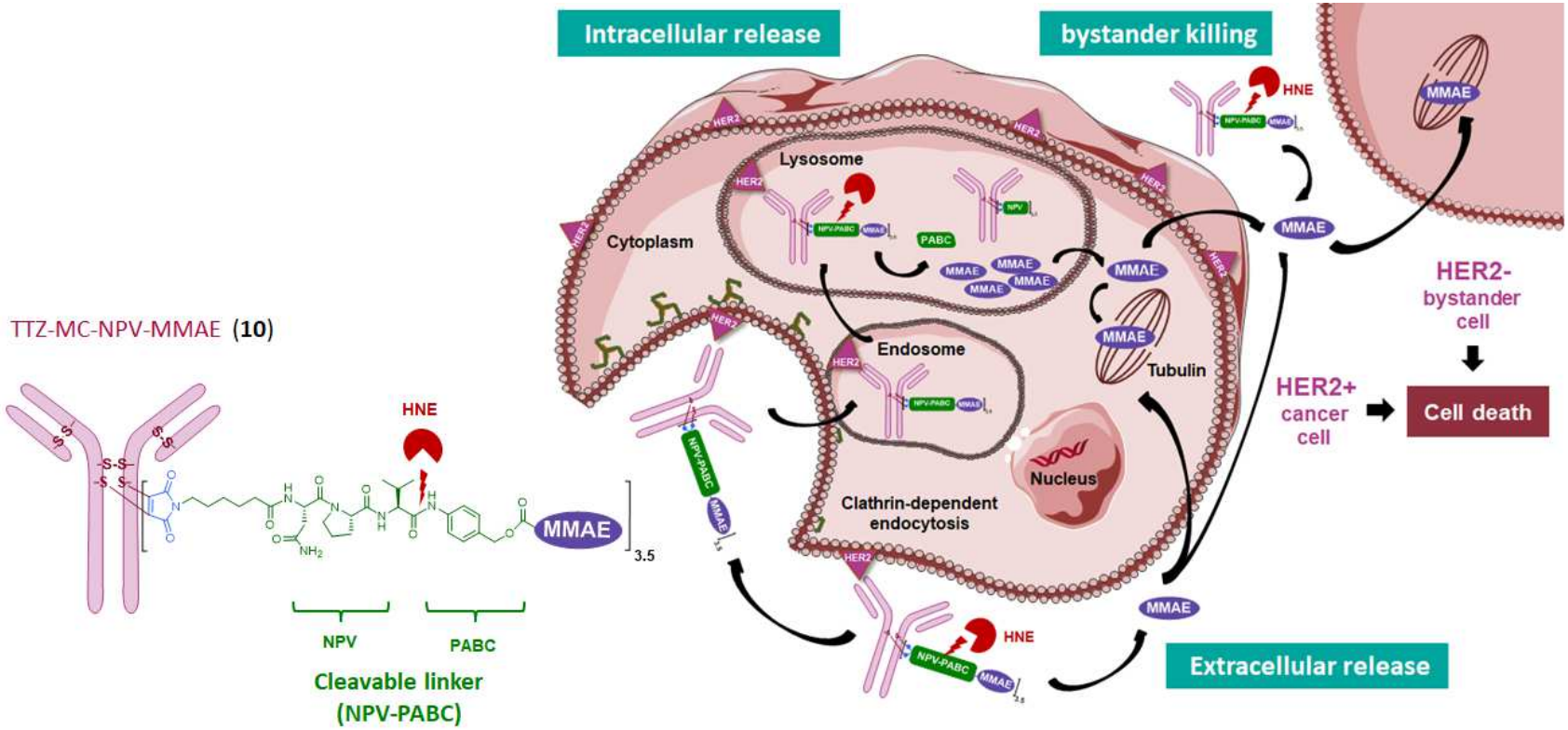

834
835
836 **Fig. 5.** Proposed mechanism of action for TTZ-MC-NPV-MMAE (**10**).

837
838
839

Intracellular release

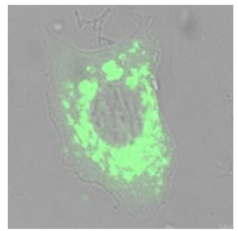

bystander killing

TTZ-MC-NPV-MMAE (**10**)

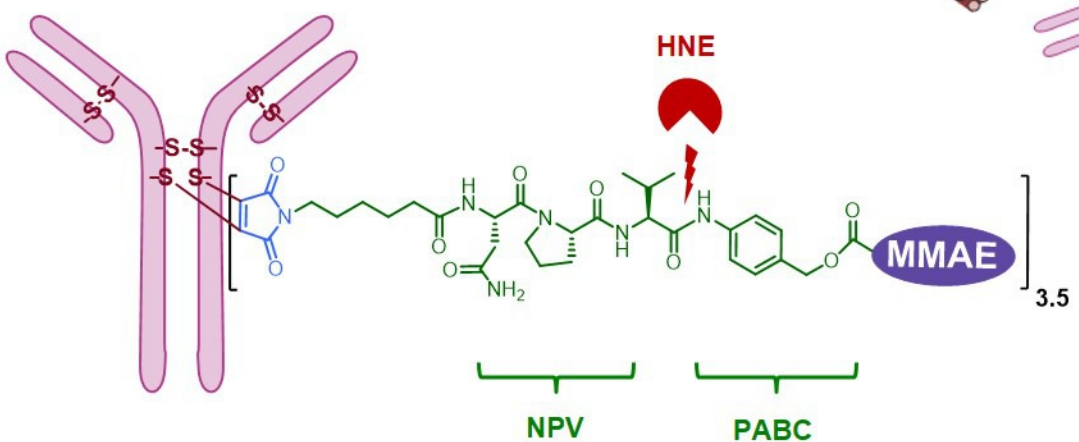

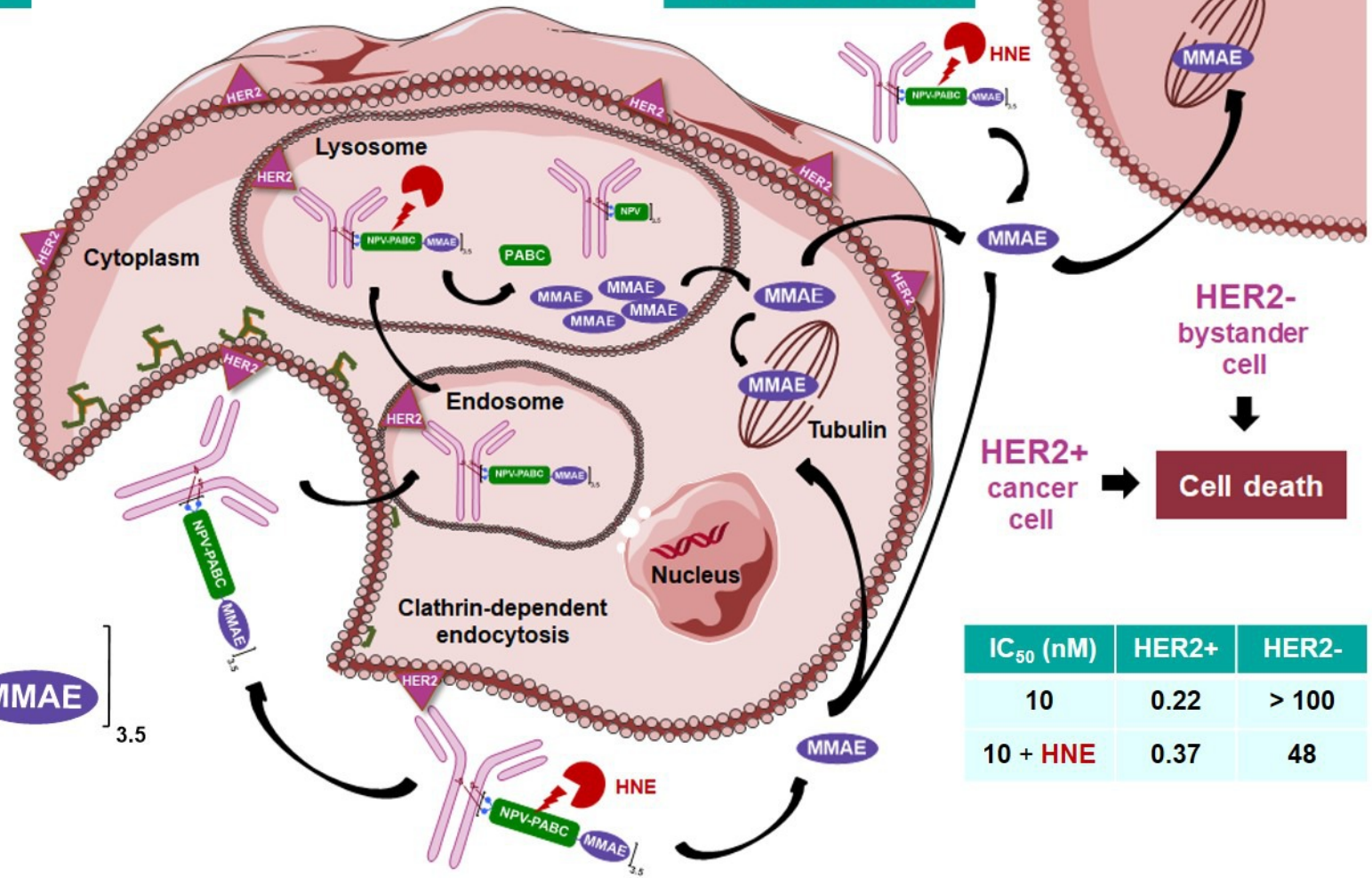

IC_{50} (nM)	HER2+	HER2-
10	0.22	> 100
10 + HNE	0.37	48

Extracellular release